J Mater Sci: Mater Med (2012) 23:2697–2708
DOI 10.1007/s10856-012-4720-5

Polyethylenimine functionalized magnetic nanoparticles as a potential non-viral vector for gene delivery

Yangbo Zhou · Zhaomin Tang · Chunli Shi · Shuai Shi · Zhiyong Qian · Shaobing Zhou

Received: 13 March 2012 / Accepted: 7 July 2012 / Published online: 24 July 2012

Abstract Polyethylenimine (PEI) functionalized magnetic nanoparticles were synthesized as a potential non-viral vector for gene delivery. The nanoparticles could provide the magnetic-targeting, and the cationic polymer PEI could condense DNA and avoid in vitro barriers. The magnetic nanoparticles were characterized by Fourier transform infrared spectroscopy, X-ray powder diffraction, dynamic light scattering measurements, transmission electron microscopy, vibrating sample magnetometer and atomic force microscopy. Agarose gel electrophoresis was used to asses DNA binding and perform a DNase I protection assay. The Alamar blue assay was used to evaluate negative effects on the metabolic activity of cells incubated with PEI modified magnetic nanoparticles and their complexes with DNA both in the presence or absence of an external magnetic field. Flow cytometry and fluorescent microscopy were also performed to investigate the transfection efficiency of the DNA-loaded magnetic nanoparticles in A549 and B16-F10 tumor cells with (+M) or without (−M) the magnetic field. The in vitro transfection efficiency of magnetic nanoparticles was improved obviously in a permanent magnetic field. Therefore, the magnetic nanoparticles show considerable potential as nanocarriers for gene delivery.

Y. Zhou · C. Shi · S. Zhou (✉)
School of Life Science and Engineering, Southwest Jiaotong University, Chengdu 610031, Sichuan, People's Republic of China
e-mail: shaobingzhou@swjtu.edu.cn; shaobingzhou@hotmail.com

Z. Tang · S. Zhou
School of Materials Science and Engineering, Key Laboratory of Advanced Technologies of Materials, Ministry of Education, Southwest Jiaotong University, Chengdu 610031, People's Republic of China

S. Shi · Z. Qian
State Key Laboratory of Biotherapy, West China Hospital, West China Medicine School, Sichuan University, Chengdu 610041, People's Republic of China

1 Introduction

In recent years some new techniques have been developed for cancer treatment, such as targeted therapy, thermal therapy and gene therapy [1–3]. Among those, gene therapy has gained significant attention as a potential method for the treatment of many inheritable or acquired diseases that are currently considered incurable. Meanwhile it is becoming thought of as a potential alternative therapy to traditional chemotherapy used for treating cancer [4, 5].

Gene delivery is one of the critical steps for gene therapy. Although viral vectors have been proven to possess high gene transfection efficiency, they have disadvantages such as immunogenicity, potential of insertional mutagenesis in the host genome, limited DNA delivery capacity and scale of production [6]. On the other hand, non-viral vectors, as promising alternatives to viral vectors for their advantages, will elicit much less immune responses or randomly integrate DNA into the host genome [7]. To date, the non-viral vectors have been widely developed and can be mainly divided into two large groups: one is organic component carriers such as cationic lipids [8, 9], polymers [10–13], peptides [14, 15] and carbon nanotubes [16]; the other is inorganic component nanoparticles such as quantum dots [17], gold nanoparticles [18], calcium phosphate particles [19] and magnetic nanoparticles [20].

Cationic polymer is an idea alternative as a vector for DNA with negative charges since they can be easily banded together by virtue of their electrostatic interactions. One of the most prominent examples among cationic polymers is

polyethylenimine (PEI), which is often considered as the gold standard of gene transfection [5, 21–23]. Its high charge density of primary, secondary and tertiary amines allows PEI to bind and compact DNA into nanoparticles, thereby it can be protected from nuclease degradation. As a result of the high density of amines, PEI lends itself to protonation with the charge density proportional to the pH of the biological environment [24]. The transfection efficiency of PEI depends on its molecular weight. High molecular weight PEI has high gene transfection efficiency but high cytotoxicity. So it is necessary to reduce the cytotoxicity of PEI and improve gene's uptaking in cancer gene therapy.

One of the key factors affecting efficiency in gene delivery is the low amount of DNA that manages to reach the target cells [25]. In this regard, the development of non-viral vectors which can be directed selectively towards specific cells is very important, and thus could improve significantly the chance of gene expression [25]. Magnetic nanoparticles generally applied in targeted drug delivery can be guided through the use of an applied magnetic field to specific tissues, organs, or possibly even into cells, allowing to reduce a considerable dose of DNA to inject and the time necessary to reach the desired target cells, enhancing significantly gene expression efficiency [26]. However, primary magnetic nanoparticles aggregate easily as a result of their large surface energy and the interaction between dipoles, which will bring a negative effect on their application in drug delivery. To resolve this problem two modifications such as physical adsorption method [27–29] and chemical conjugation method [30–32] have been developed to tailor magnetic nanoparticle surface with biocompatible polymers.

In the study, the chemically modified magnetic nanoparticles with surface positive charges were investigated as a non-viral vector for gene delivery to reduce toxicity and increase the transfection efficiency with a permanent magnetic field. The nanoparticles comprised of superparamagnetic iron oxide nanoparticles (SPIONs) chemically conjugated with PEI. The functionalized nanoparticles with smaller size are stable in the water due to the chemical bonds between magnetic nanoparticles and PEI. The SPIONs would provide the magnetic-targeting, and the cationic polymer PEI could carry with DNA and avoid in vitro barriers for gene delivery. The transfection efficiency of the DNA-loaded magnetic nanoparticles was investigated in A549 and B16-F10 tumor cells with (+M) or without (−M) the magnetic field.

2 Materials and methods

2.1 Materials

Ferrous chloride tetra-hydrate ($FeCl_2{\cdot}4H_2O$), ferric chloride hexahydrate ($FeCl_3{\cdot}6H_2O$) iron salts, aqueous ammonium hydroxide (25–28 %, w/w), Sodium citrate (CA) and *N*-hydroxysulfosuccinimide (sulfo-NHS) were purchased from Chengdu KeLong Chemical Reagent Company (Sichuan, China) and used as received. Polyethylenimine branched (PEI, Mn 25000) was purchased from Aldrich (USA). *N*-(3-dimethylaminopropyl)-*N*′-ethylcarbodiimide hydrochloride (EDC) was purchased from Pierce (Rockford, IL, USA).

The osteoblasts belonged to normal cell line, which was from neonatal rat's skull. The A549 (the human alveolar epithelial cell line) and B16-F10 (the mouse melanoma cell line) cells, the plasmid DNA and the plasmid of green fluorescent protein (GFP) were presented by Sichuan University (China). Permanent magnetic field was provided by permanent magnets placed directly underneath the cell culture plate. The magnetic field strength was measured by Gaussmeter (HT 201 Hengtong magnetoelectricity Co., Ltd, China), and the magnetic field strength M = 0.1 T.

2.2 Synthesis of PEI functionalized magnetic nanoparticles (SPIONs@PEI)

The synthesis of SPIONs@PEI can be divided into two steps as shown in Scheme 1. Firstly, SPIONs@CA was prepared by modified chemical co-precipitation as our previous report [33]. In brief, 4.1 g ferric chloride hexahydrate, 1.791 g ferrous chloride tetra-hydrate (molar ratio: 2:1) and 100 mL distilled water were added in a three-necked flask with gently stirring. After the mixture solution dissolved completely, 25 mL aqueous ammonium hydroxide (25–28 %, w/w) and 8.823 g CA were added with vigorous stirring under the protection of nitrogen atmosphere at 80 °C for 1 h and then cooled down to the ambient temperature. After reaction, the precipitate SPIONs@CA was collected by a magnet and washed five times with distilled water. Finally, SPIONs@CA aqueous solution was freeze-dried and stored at 4 °C for further use.

Secondly, SPIONs@PEI was synthesized via amide reaction between terminal amino groups of PEI and carboxyl groups of CA located on the surface of SPIONs. The mixed solution containing 200 mg PEI and 100 mg SPIONs@CA dissolved in 30 mL distilled water was activated by adding 70 mg of EDC and 120 mg *N*-hydroxysuccinimide (NHS). The mixture was magnetically stirred for 48 h at ambient temperature. The following procedures were similar with the fabrication of SPIONs@CA referred above. SPIONs@PEI/DNA complex can be obtained by mixing SPIONs@PEI solution with DNA solution.

2.3 Characterization

The Fourier transform infrared spectroscopy (FT-IR, Nicolet, 5700) was performed to analyze the surface

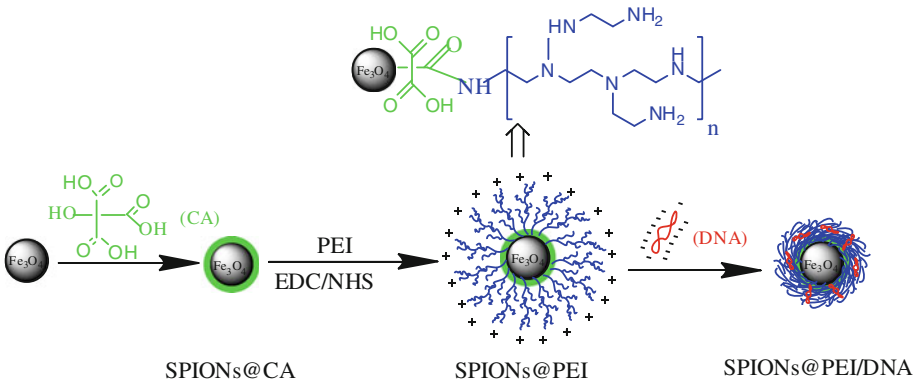

Scheme 1 Scheme of synthesis of SPIONs@PEI/DNA complex

functionalization of all samples. The modified nanoparticles were analyzed for phase composition using X-ray powder diffraction (XRD, Philips, X'Pert PRO) over the 2θ range from 10° to 90° at rate of 2.5° min^{-1}, using Cu-Kα radiation ($\lambda = 1.54060$ Å) at room temperature. The magnetic properties were measured with a vibrating specimen magnetometer (VSM, Lake Shore 7410) under the conditions of 300 K, 1000 A m^{-1} and 16 Hz at room temperature. Particle size, distribution and Zeta Potential were determined by Particle Size Analyzer (ZETA-SIZER, MALVERN, Nano-ZS90). The morphology and size were observed by using transmission electron microscopy (TEM, HITACHI, H-700H) at an accelerating voltage of 175 kV and atomic force microscopy (AFM, CSPM5000, Being, China).

2.4 Stability of SPIONs@PEI

The UV–Visible spectrophotometry (UV-2550, Shimadzu, Japan) was employed to investigate the stability of SPIONs@PEI in the various external environments. In the presence of NaCl at a concentration of up to 500 mM, the stability was firstly evaluated. The magnetic nanoparticles were centrifuged (Anke TGL-16B, Shanghai) at 5,000 rpm for 0, 1, 3, 5, 7, 9, 12 and 15 min, respectively, and the absorbance of the solution was recorded periodically as previous report [34]. Furthermore, the stability of SPIONs@PEI was further studied at pH 2–12 and at temperatures from 25 to 41 °C. The stability of the magnetic nanoparticles in the presence of serum was also evaluated at different period of time.

2.5 Acid–base titration

The buffer capabilities of PEI, and SPIONs@PEI were determined by acid–base titrations over the pH ranging from 10.0 to 2.8. In brief, each sample solution of 0.2 mg mL^{-1} was mixed in 30 mL of 150 mM NaCl solution before titration. Firstly, the sample solution was titrated by 0.1 M NaOH until the pH values reach to 10. Secondly, different volumes of 0.1 M HCl were added into the solution with gently stirring. During the experiment period, the different pH values were measured by using a pH meter. And 150 mM NaCl solution was used as control.

2.6 Determination of particle size and zeta potential of SPIONs@PEI/DNA complexes

Zeta potential and particle size of SPIONs@PEI/DNA complexes were evaluated using Particle Size Analyzer (ZETA-SIZER, MALVERN, Nano-ZS90). SPIONs@PEI/DNA complexes were prepared in water at various N/P ratios. Before measurement, the complexes were incubated at room temperature for 15 min.

2.7 DNA binding assay

The capability of condensing negatively charged nucleonic acid and protecting DNA from degradation were measured by the agarose gel electrophoresis. Firstly, the 0.1 mg mL^{-1} plasmid DNA and the SPIONs@PEI were mixed with the same volume at different N/P ratios and vortexed shortly. After 15 min incubation at room temperature, 10 μL mixture solution was determined by 1 % agarose gel electrophoresis (90 V, 30 min). And the naked DNA was used as control.

2.8 DNase I protection assay

SPIONs@PEI/DNA nanoparticles at various N/P ratios and naked DNA (0.3 μg) were incubated for 15 min at 37 °C with DNase I (1 unit) in DNase/Mg^{2+} digestion buffer consisting of 50 mM Tri-Cl, pH 7.6 and 10 mM $MgCl_2$. The DNase I was then inactivated by adding 4 μL of 250 mM ethtylenediaminetetraacetic acid (EDTA) (pH = 8) and incubated for 15 min at room temperature. 2 μL of 1 mg mL^{-1} of sodium heparin was added to release the DNA from the complex nanoparticles for 2 h.

The DNA integrity was assessed by 1 % agarose gel electrophoresis (90 V, 30 min). And the naked DNA was used as control.

2.9 Cytotoxicity and cellular uptake of the magnetic nanoparticles

Alamar blue assay as a metabolic test has gained popularity as a very simple and versatile method of measuring cell cytotoxicity and metabolic activity. The Alamar blue agents is non-toxic, so continuous monitoring of cultured cells is permitted. Osteoblasts were cultured in DMEM medium supplemented with 10 % fetal bovine serum (FBS) at 37 °C in a 5 % CO_2 incubator. And B16-F10 cells were cultured in RPMI 1640 medium supplemented with 10 % FBS at 37 °C in a 5 % CO_2 incubator. For the cytotoxicity test, osteoblasts and B16-F10 cells were seeded of distinction in 24-well tissue culture plates at a density of 1×10^4 cells per well in medium with (+M) and without (−M) a permanent magnetic field.

For magnetic nanoparticle cytotoxicity assay, after the cells cultured 24 h, the culture medium was replaced with 1.5 mL of medium containing the various concentrations of PEI, SPIONs@CA and SPIONS@PEI were added to each well. The Alamar blue assay was performed after one day's culture.

For magnetic nanoparticles/DNA cytotoxicity assay, after the cells cultured 24 h, magnetic nanoparticles were complexed with 2 μg DNA at different N/P ratios for 30 min, which was the same as transfection conditions. After that, the complexes were added to each well. After the complexes were added for 4 h, the medium was replaced with 200 mL of fresh medium and cultured 24 h. The naked DNA and PEI/DNA were used as control.

Followed the above steps, each well was washed twice with PBS, and then added with 280 μL Medium 199 (Ml99), 10 μL FBS, and 10 μL Alamar blue agents. The cells were incubated at standard cell culture conditions for 4 h with a color change from indigo blue to pink. Then the optical absorbance of the medium was read at 570 and 600 nm (mQ × 200, BIO-TEK, USA) against a medium-blank with Alamar blue.

The cellular uptake of magnetic nanoparticles analysis was also performed. Prussian blue staining was used to reveal the presence of iron cations in the Osteblastos and B16-F10 cells with (+M) or without (−M) a permanent magnetic field. The cells were fixed with 2.5 % glutaraldehyde and washed with PBS, followed by incubation with 2 % potassium ferrocyanide in 6 % hydrochloric acid for 3 h. After wash, they were counterstained with neutral red solution. The samples were then examined under an optical microscopy (Olympus IX51, Japan).

To quantify the intracellular uptake of the nanoparticles, the seeding of B16-F10 and the incubation with the nanoparticles were carried out as follows. Cells were seeded at the cell density of 1×10^5 cells per well in a 6-well plate and grown in a 2 mL medium for 24 h. The culture medium was replaced with a medium containing the nanoparticles. After 6 h, the cells were washed three times with PBS, detached, resuspended, counted, and centrifuged down. Then, the cells were dissolved in a 37 % HCl solution at 80 °C for 30 min. The intracellular iron concentration was quantified using AAS (Polarized Zeeman Atomic Absorption Spectrophotometer HITACHI Z-5000) [35].

2.10 In vitro transfection

Transfection of GFP plasmid mediated SPIONs@PEI/DNA in A549 and B16-F10 cells was evaluated at various N/P ratios. PEI/DNA, Lipofectamine 2000/DNA and naked DNA complexes were performed as control. Experiments were performed in 6-well plates at a beginning cell density of 1×10^5 cells per well and incubated at 37 °C for 24 h. After that, the complexes in 2 mL serum-free RPMI 1640 medium were added to each well, the cells were incubated at 37 °C for 4 h in a humidified atmosphere with 5 % CO_2. Magnetofection was performed by applying a permanent magnetic field (+M) during the transfection period of the original 15 min. Afterwards, the media was replaced with fresh RPMI 1640 containing 10 % FBS and incubated for an additional 24 h at 37 °C. Then the cells were digested by Trypsin, centrifuged down, washed three times with PBS, resuspended to make the cell density of 1×10^6 mL^{-1}. The transfection efficiency was monitored by using flow cytometry by taking up FITC channel (Epics Elite EST, USA) and was visualized by fluorescence microscopy (Olympus IX71, Japan).

To study the effect of serum on transfection efficiencies, the RPMI 1640 containing 10 % FBS was used to transfect cells with SPIONs@PEI/DNA complexes. Prior to transfection, when the cells achieved 50 % confluence, the medium was replaced with fresh RPMI 1640 containing 10 % FBS, and then, SPIONs@PEI/DNA complexes at N/P ratio of 9 was added to each well. The other procedure was the same as described above.

3 Results

3.1 Characterizations of SPIONs@PEI

The structures of SPIONs@CA and SPIONs@PEI are confirmed by FT-IR as shown in Fig. 1a. In the up line, the peak at about 1,710 cm^{-1} is related to the asymmetric vibration of C=O in carboxyl group of CA. And the peak at about 595 cm^{-1} is due to the vibration of Fe–O. In the

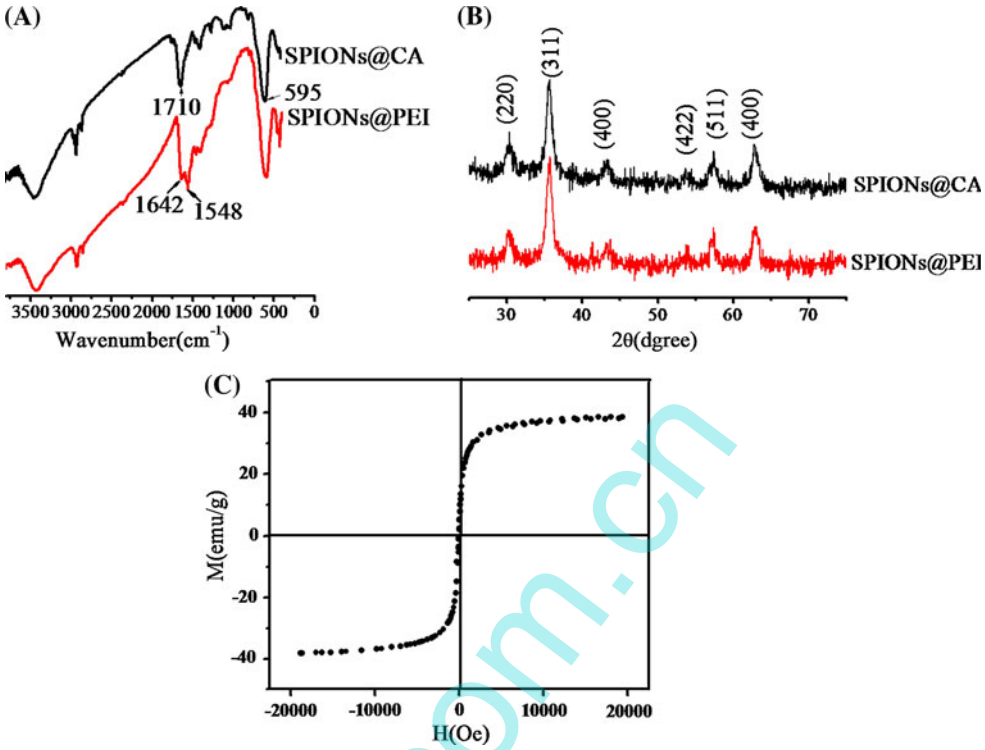

Fig. 1 FT-IR spectrums (**a**), XRD patterns (**b**) and hysteresis loops of the SPIONs@PEI (**c**)

down line, the peaks at 1,642 and 1,548 cm^{-1} are due to the amido bonds in the SPIONs@PEI. The XRD of the CA and PEI coated magnetic nanoparticles are shown in Fig. 1b, six characteristics peaks for Fe_3O_4 marked by their indices (2 2 0), (3 1 1), (4 0 0), (4 2 2), (5 1 1), and (4 4 0) are observed for both samples as the characteristic peaks of standard Fe_3O_4 crystal plane according to JCPDS [85-1436], which indicates that each sample is Fe_3O_4 crystals with cubic spinel structure and the incorporation of polymer to SPIONs does not influence Fe_3O_4 crystallization. VSM analysis demonstrates the magnetization behavior versus applied magnetic field for SPIONs@PEI (Fig. 1c). The saturation magnetization level of SPIONs@PEI is comparable at 38.1 emu g^{-1}. The absence of a hysteresis loop with reversal of the magnetic field indicates that there is no magnetic energy loss, which is consistent with superparamagnetic behavior.

TEM and AFM are used to observe the morphology of SPIONs@CA and SPIONs@PEI. As shown in Fig. 2a–d, SPIONs@CA and SPIONs@PEI possess excellent dispersibility in water, which suggests that the CA and PEI molecules immobilized on SPIONs could improve the nanoparticle dispersion in water as a result of steric repulsion forces. The TEM photo in Fig. 2b shows that SPIONs@PEI aggregated a little in aqueous phase. Furthermore, Fig. 2e exhibits that the z-average diameter values of SPIONs@CA and SPIONs@PEI are 68 and 165 nm, respectively. Figure 2f displays that the zeta potential value transformed from negative (−31.8 mv) to positive values (+22.5 mv).

3.2 The stability of SPIONs@PEI

The stability of SPIONs@PEI dispersed in the aqueous solution was studied in specific environments. The absorbance of the magnetic nanomicelles at 350 nm was recorded and illustrated in Fig. 3 based on previous report [36]. As seen from Fig. 3a, after SPIONs@PEI are treated with NaCl with various concentrations from 0 to 500 mM, the absorbance almost kept constant, indicating that the SPIONs@PEI solution is very stable [37]. Figure 3b displays that no significant change in absorbance is observed after SPIONs@PEI were centrifuged in different time periods, which suggested that SPIONs@PEI was reasonably stable under this condition. Furthermore, the stability of the magnetic nanoparticles was further studied at pH 2–12. Similarly, the absorbance of SPIONs@PEI has no significant change (Fig. 3c). In addition, the absorbance of SPIONs@PEI at different temperatures from 25 to 41 °C are monitored, and the absorbance has no obvious change (Fig. 3d). To confirm that the magnetic nanoparticles can be used in vivo, the stability was also conducted in the presence of serum at different period of time. The results indicate that stable dispersion occurred due to the steric repulsion among PEI chains and the repulsion of positive charges. It is seemed that the dispersion and stability are

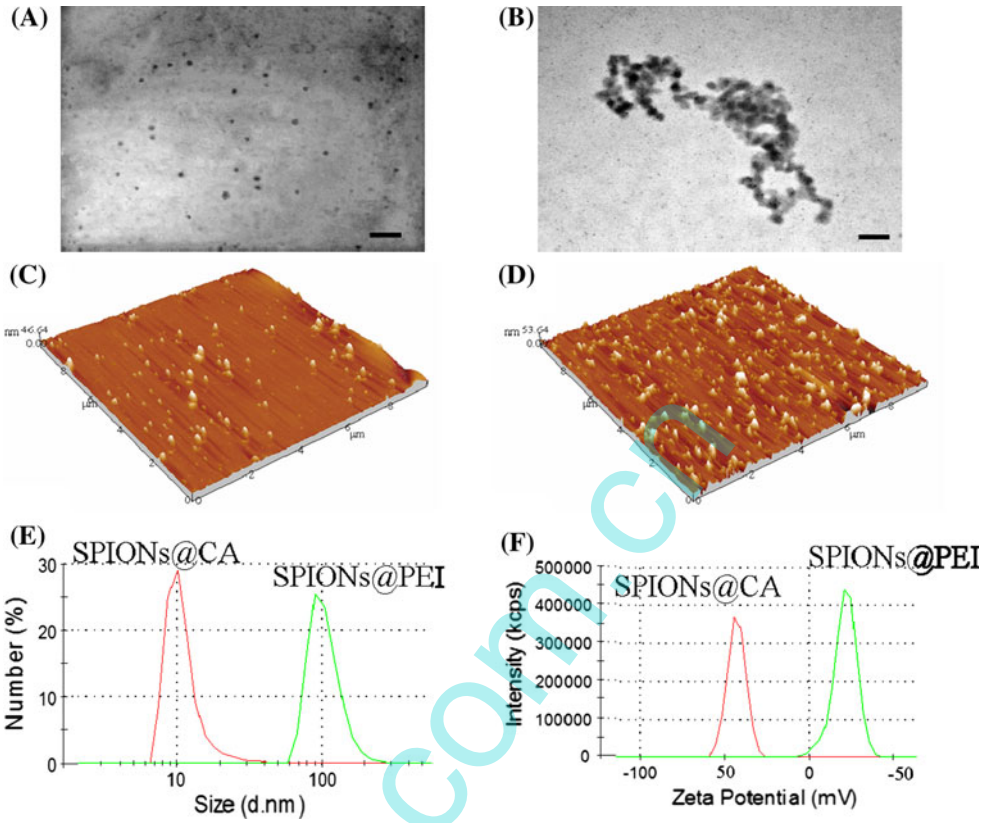

Fig. 2 TEM images of SPIONs@CA (**a**), SPIONs@PEI (**b**) (scale bar, 100 nm), AFM images of SPIONs@CA (**c**), SPIONs@PEI (**d**), size distribution (**e**) and Zeta potential (**f**) of SPIONs@CA and SPIONs@PEI

strongly influenced by the PEI grafted on the nanoparticles surface [32].

3.3 Acid–base titration

Acid–base titration was executed to monitor the buffering capability of SPIONs@PEI. As seen from Fig. 4, we can find that the difference in the buffering capability between the samples of PEI and the magnetic nanoparticles chemically conjugated PEI is little, indicating that SPIONs@PEI can be applied as a potential non-viral vector in gene delivery.

3.4 Determination of particle size and zeta potential of SPIONs@PEI/DNA complexes

The size and zeta potential of SPIONs@PEI/DNA complex are important factors for cell uptake [38]. The hydrodynamic sizes of SPIONs@PEI bound with DNA at different N/P ratios were determined using dynamic light scattering (DLS) as displayed in Fig. 5A. SPIONs@PEI/DNA formed at a ratio of 3:1 have a size of 230 ± 6 nm, while the size decreases to 209 ± 22 nm at a ratio of 6:1. The size increases as the N/P ratio further increases, and remains stable for higher ratios. The zeta potential of SPIONs@PEI/DNA complex not only determines the nanoparticles stability but also influences the interaction with negatively charged cell membranes, and further impacts the transfection efficiency. Figure 5A shows the zeta potentials of SPIONs@PEI/DNA complexes as a function of SPIONs@PEI/DNA ratio. It was noted that all the sharp changes in size occurred at SPIONs@PEI/DNA ratios when the zeta potential underwent a transition from negative to positive values. The large positive zeta potential and DNA protection provided by SPIONs@PEI suggest that it might provide a high transfection efficiency. SPIONs@PEI/DNA has negative zeta potentials at low N/P ratios but becomes positively charged at a ratio of 6:1 and above.

3.5 DNA binding assay

To determine the optimal binding of SPIONs@PEI with DNA, we analyzed the DNA mobilities after binding by gel electrophoresis. Figure 5B(a) shows agarose gel electrophoresis of SPIONs@PEI/DNA complexes at various N/P ratios, and naked DNA used as control. The N/P ratios of SPIONs@PEI/DNA were 3, 6, 9, 12, and 15, respectively, where the content of DNA was kept at 0.3 μg. In contrast to the naked plasmid DNA, the migration of plasmid was completely blocked at the N/P ratio of 9:1. We can

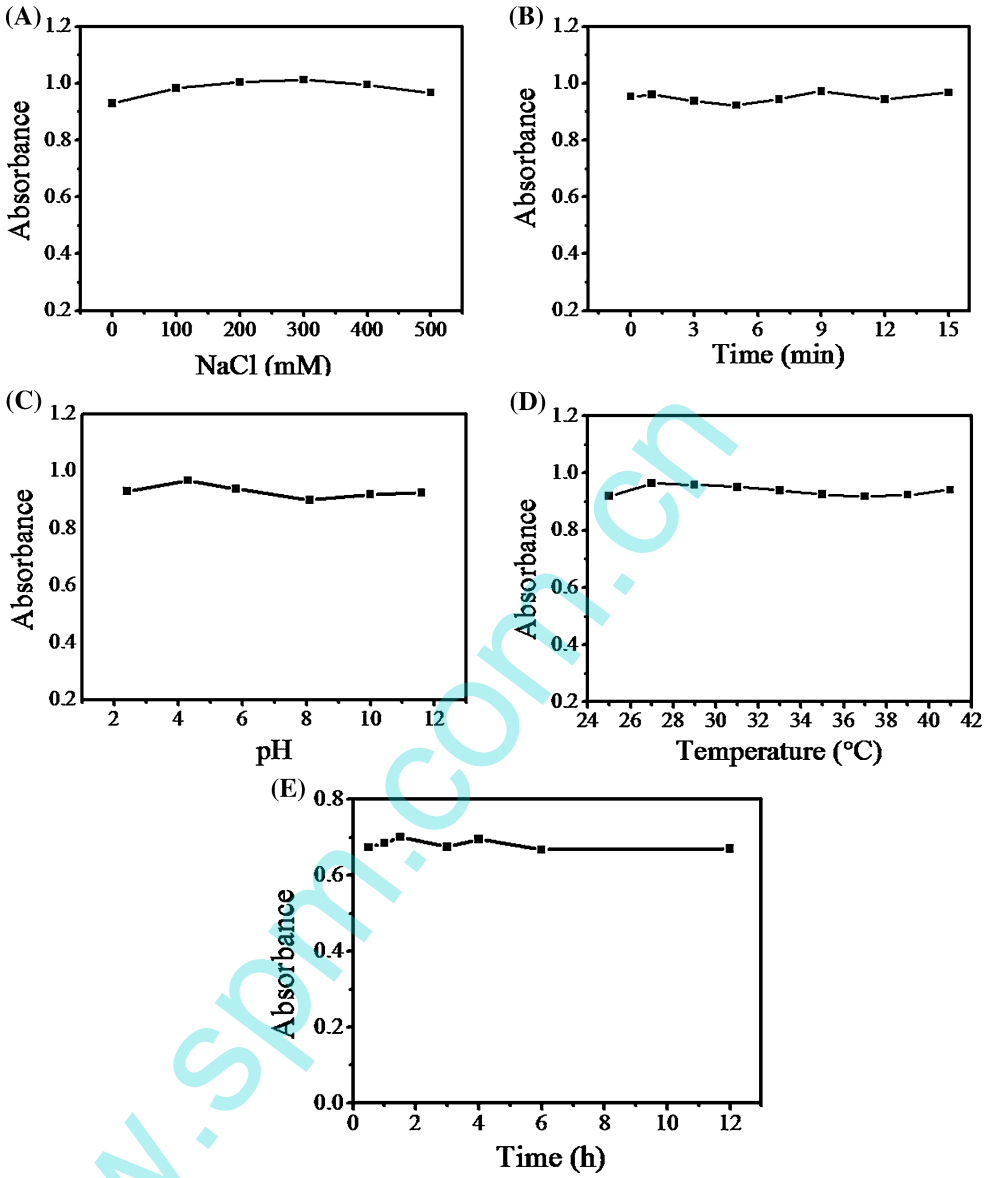

Fig. 3 The absorbance changes at 350 nm of SPIONs@PEI as functions of the addition of NaCl aqueous solution with various concentrations (**a**), centrifugal time (**b**), pH values (**c**), temperatures (**d**), and in the presence of serum at different period of time (**e**)

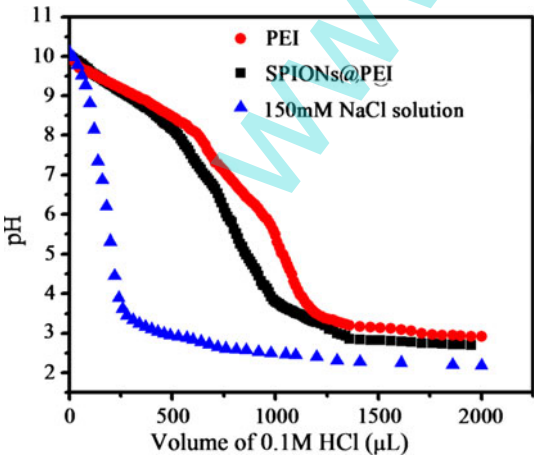

Fig. 4 The buffering capacity of PEI, SPIONs@PEI and 150 mM NaCl solution

conclude that SPIONs@PEI nanoparticles can concentrate DNA at N/P ratio of 9:1.

3.6 DNase I protection assay

In Fig. 5B(b) the capability of protecting plasmid DNA from DNase degradation was examined using DNase I as model enzyme. After incubated with DNase I in DNase/Mg^{2+} digestion buffer at 37 °C for 20 min, naked plasmid DNA showed significant degradation, while the plasmid DNA released from SPIONs@PEI/DNA complexes (N/P = 9:1) remained intact. The results of DNase I protection assays show that the SPIONs@PEI are able to effectively protect DNA from DNase I digestion, thus implying application prospects to a certain extent.

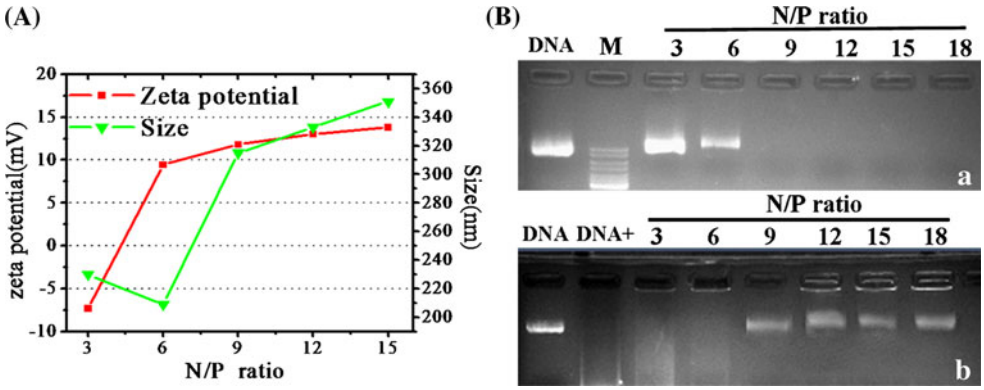

Fig. 5 Zeta potential and particle size of SPIONs@PEI/DNA nanoparticles at various N/P ratios (**A**), Agarose gel electrophoresis of SPIONs@PEI/DNA complexes at various N/P ratios (**B**(*a*)) and Electrophoretic mobility analysis of SPIONs@PEI/DNA nanoparticles after DNase I treatment (**B**(*b*))

3.7 Cytotoxicity and the cellular uptake of magnetic nanoparticles analysis

To evaluate the toxicity of SPIONs@PEI and its DNA complexes, the cell viabilities of two different cell lines, osteoblasts and B16-F10 were tested by Alamar blue assay. Figure 6a, b shows that SPIONs@CA maintain relatively high cell viabilities (more than 95 %) in all cell lines with (+M) and without (−M) a magnetic field. The cell viability of SPIONs@PEI is decreased more obviously than SPIONs@CA at the same concentration, which can be ascribed to a surface charge transition from negative to positive values. However, we can also find that SPIONs@PEI exhibits low cytotoxicity at lower concentration, and at the same concentration the cell viability of SPIONs@PEI with the magnetic field is lower than that no magnetic field, also suggesting that the cellular uptake of SPIONs@PEI with the magnetic field is more than that with no magnetic field. In particular, the cytotoxicity of SPIONs@PEI was much less than pure PEI at the same concentration. The reason is that the magnetic nanoparticles possess better biocompatibility than cationic PEI and thus the incorporation PEI into the nanoparticles can decrease the toxicity of PEI. Therefore, the evaluation of cytotoxicity of SPIONs@PEI/DNA complex represented that the complex was of minimal toxicity as shown in Fig. 6c, d. It can also be found that there was more than 90 % cell viability at N/P ratios from 3 to 9 with and without the magnetic field, moreover, the lower N/P ratio complexes presented slighter toxicity. Furthermore, the cell viability of SPIONs@PEI/DNA complexes was higher than PEI/DNA complexes with less than 75 % cell viability at the optimal N/P ratio.

To examine the cellular uptake of magnetic nanoparticles in osteoblasts and B16-F10 cells, the prussian blue staining was carried out. SPIONS@CA and SPIONs@PEI appear blue due to the formation of prussian blue precipitates inside the cells as displayed in Fig. 6e, indicating that SPIONs@CA and SPIONs@PEI were internalized into the cells via endocytosis. Simultaneously, the blue color inside osteoblasts and B16-F10 cells were clearer in the presence of SPIONs@PEI than SPIONs@CA, suggesting that the larger amount of iron oxides was uptaken. It can be also explained that more nanoparticles with positive charges could enter the cells via the electrostatic interaction with negatively charged cell membrane [39]. And the area of blue colour for both SPIONs@CA and SPIONs@PEI in the magnetic field appeared bigger than those without magnetic field, which demonstrated that the cellular uptake of the magnetic nanoparticles could be assisted by the magnetic field. Figure 6f shows the quantification of the uptake of SPIONs@CA and SPIONs@PEI by B16-F10 cells when cultured in medium containing the nanoparticles with (+M) and without (−M) a permanent magnetic field. The iron uptake of SPIONs@PEI is higher than that of SPIONs@CA under the same condition. The iron uptake of both SPIONs@CA and SPIONs@PEI was higher with the magnetic field than that with no magnetic field.

3.8 In vitro transfection

The transfection activity mediated by SPIONs@PEI was also assessed in A549 and B16-F10 cells respectively. In the luciferases analysis, the plasmid GFP was used as a reporter gene, PEI was used as a control reagent. After transient transfection and additional incubation for 24 h, the transfection efficiency was quantitatively analyzed using flow cytometry. As shown in Fig. 7A, the highest transfection efficiency (37.5 %) is observed in B16-F10 cell line for SPIONs@PEI/DNA complex while the efficiency of Lipofectamine 2000/DNA and PEI/DNA complex were 35.3 and 30.0 % respectively with a magnetic field, and the efficiency of naked DNA was almost equal to 0. Moreover, the transfection activity of SPIONs@PEI/DNA in the presence of a magnetic field was higher than that with the absence of a magnetic field at the same N/P ratio. And the same situations occurred in A549 cell lines (Fig. 7B). Figure 7C shows the transfection efficiency of SPIONs@PEI/DNA in B16-F10 cells in the presence of 10 % serum. Among all the SPIONs@PEI/DNA showed the transfection efficiency was two-fold higher in the

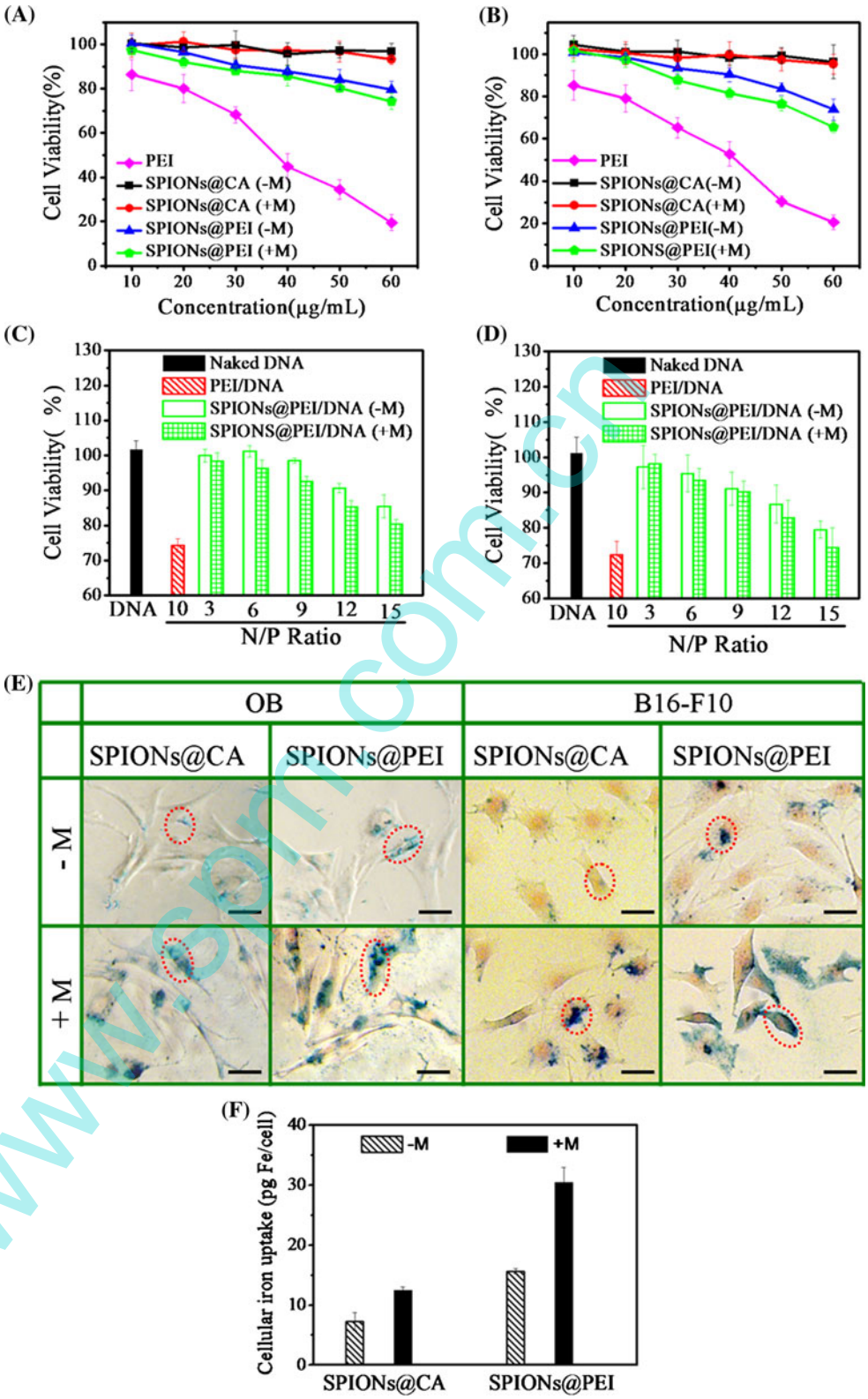

Fig. 6 Cell viability of osteoblasts (**a**) and B16-F10 (**b**) on the different concentrations of PEI and the SPIONs@PEI, cell viability of osteoblasts (**c**) and B16-F10 (**d**) of SPIONs@PEI/DNA at the different N/P ratios and Prussian blue staining (**e**) of osteoblasts and B16-F10 cells after 6 h incubation with SPIONs@PEI without (−M) or with (+M) the magnetic field (scale bar, 2 μm) and the quantification of uptake (**f**) of SPIONs@CA and SPIONs@PEI by B16-F10 cells

presence of a magnetic field than that no magnetic field. Additionally, the presence of serum has no obvious influence on the transfection efficiency under the magnetic field. Similar results were obtained in A549 cells (Fig. 7D). The transfection efficiency in B16-F10 and A549 at N/P ratio of 9:1 is shown in the flow cytometry graphs

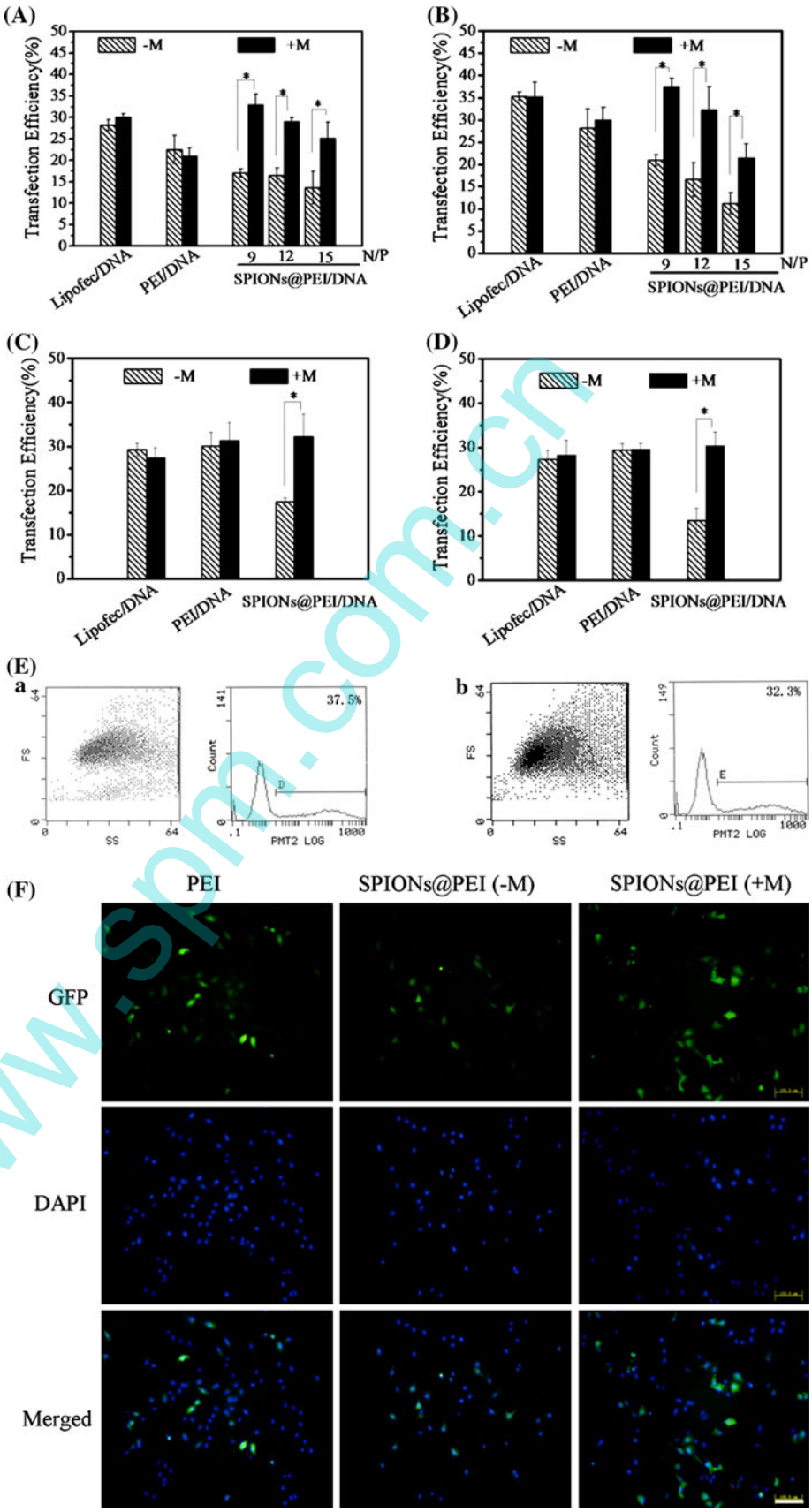

Fig. 7 The transfection efficiency in B16-F10 (**A**) and A549 (**B**) cell lines cocultured with SPIONs@PEI at the various N/P ratios combined with DNA in the absence of 10 % FBS; the transfection efficiency in B16-F10 (**C**) and A549 (**D**) cell lines at N/P ratios of 9 in the presence of 10 % FBS. Both (**A**), (**B**) and (**C**), (**D**) used Lipofectamine 2000/DNA and PEI/DNA as control. And the transfection efficiency was demonstrated by the flow cytometry data ($^*P < 0.05$, n = 3); the flow cytometry graphs of the transfection efficiency (**E**) in the two cell lines: (*a*) B16-F10 and (*b*) A549 at N/P ratio of 9:1 without 10 % FBS; Fluorescent microscopic images (**F**) of GFP expressed A549 cells (scale bar, 100 μm)

(Fig. 7E). The decrease of the transfection efficiency at higher N/P ratios could be attributed to the higher cytotoxicity of materials.

The transfection efficiency can also be directly visualized with a fluorescent microscopy when GFP is used as the report gene. Figure 7F shows that the cells transfected by SPIONs@PEI/DNA complex with the magnetic field express more green fluorescent proteins than that without the magnetic field. Additionally, the transfection efficiency with the magnetic field showed significant statistical difference compared with no magnetic field in B16-F10 cells ($P < 0.05$), and A549 cells followed the same rules. It reveals that SPIONs@PEI/DNA complex could be employed as a more effective vector to deliver larger amount of plasmids in the presence of a magnetic field than that with no magnetic field.

4 Discussion

It is of great importance to optimize the stability of the magnetic nanoparticles dispersed in water, which is a basic requirement for their application as nanocarriers in gene delivery. Nanoparticles have high stability in the physiological environment and small size to allow a long blood circulation [40]. SPIONs@PEI nanoparticles show good stability in the general environment even in electrolyte solution, which is very important for in vivo and clinical applications. The branched form of PEI contains the large number of amine groups, each with the potential to be protonated. This gives PEI the attribute of serving as an effective buffer through a wide pH range. It is thought that gene vectors with good buffering capability may help DNA-containing complexes escape from the endosomes and consequently promote transfection activity according to the "proton sponge" hypothesis [41]. The cytotoxicity of gene vector is crucial to the clinical application, which strongly depends on the biocompatibility of vector materials. Herein, the SPIONs@PEI nanoparticles display good biocompatibility in the presence of an external magnetic field. At the same time, the presence of the magnetic field can improve the transfection efficiency of DNA. The reason could be attributed to these effects: (1) magnet increases sedimentation rates, (2) magnet increases nanoparticle internalization, (3) the plasmid released intracellularly was improved [42].

5 Conclusion

It is very necessary to develop a non-viral gene transfer reagent with incorporation of safety to body with high transfection efficiency of therapeutic genes. In this study, PEI functionalized magnetic nanoparticles (SPIONs@PEI) were successfully fabricated for gene transfection by chemical conjugation method. The magnetic nanoparticles with an average size of 165 nm exhibited well aqueous dispersity, excellent stability and superparamagnetism. The result of Alamar blue assay displayed that the magnetic micelles were safe and effective carriers as gene delivery. The result from flow cytometry and fluorescent microscopy indicated that the transfection efficiency of the PEI functionalized magnetic nanoparticles was enhanced for B16-F10 cells and A549 cells under a permanent magnetic field and the presence of serum have little influence on it. Therefore, as safety is a primary concern in the development of nanomaterials for in vivo applications, the magnetic nanoparticles is a good candidate for gene delivery in gene therapy.

Acknowledgments This work was partially supported by National Basic Research Program of China (973 Program, 2012CB933602), National Natural Science Foundation of China (No. 30970723 and No. 51173150), Fundamental Research Funds for the Central Universities (SWJTU11ZT10) and the Open Research Fund of the Key Laboratory of Biotherapy, West China Hospital, West China Medicine School, Sichuan University under Grant No. SKLB200907.

References

1. Yao Z, Fenoglio S, Gao DC, Camiolo M, Stiles B, Lindsted T, Schlederer M, Johns C, Altorki N, Mittal V. TGF-β IL-6 axis mediates selective and adaptive mechanisms of resistance to molecular targeted therapy in lung cancer. PANS. 2010;107:15535–40.
2. Day ES, Morton JG, West JL. Nanoparticles for thermal cancer therapy. J Biomech Eng. 2009;131:074001.
3. Redd WH, Montgomery GH, DuHamel KN. Behavioral intervention for cancer treatment side effects. J Natl Cancer Inst. 2001;93:810.
4. Lungwitz U, Breunig M, Blunk T, Gopferich A. Polyethylenimine-based non-viral gene delivery systems. Eur J Pharm Biopharm. 2005;60:247–66.
5. Godbey W, Wu KK, Mikos AG. Poly (ethylenimine) and its role in gene delivery. J Controlled Release. 1999;60:149–60.
6. Thomas CE, Ehrhardt A, Kay MA. Progress and problems with the use of viral vectors for gene therapy. Nat Rev Genet. 2003;4:346–58.
7. Jackson DA, Juranek S, Lipps HJ. Designing nonviral vectors for efficient gene transfer and long-term gene expression. Mol Ther. 2006;14:613–26.
8. Floch V, Loisel S, Guenin E, Hervé AC, Clément JC, Yaouanc JJ, Abbayes H, Férec C. Cation substitution in cationic phosphonolipids: a new concept to improve transfection activity and decrease cellular toxicity. J Med Chem. 2000;43:4617–28.
9. Floch V, Legros N, Loisel S, Guillaume C, Guilbot J, Benvegnu T, Ferrieres V, Plusquellec D, Ferec C. New biocompatible cationic amphiphiles derivative from glycine betaine: A novel family of efficient nonviral gene transfer agents* 1. Biochem Biophys Res Commun. 1998;251:360–5.
10. Hobel S, Prinz R, Malek A, Urban-Klein B, Sitterberg J, Bakowsky U, Czubayko F, Aigner A. Polyethylenimine PEI F25-LMW allows the long-term storage of frozen complexes as fully

active reagents in siRNA-mediated gene targeting and DNA delivery. Eur J Pharm Biopharm. 2008;70:29–41.
11. Jiang X, Lok MC, Hennink WE. Degradable-brushed pHEMA–pDMAEMA synthesized via ATRP and click chemistry for gene delivery. Bioconjugate Chem. 2007;18:2077–84.
12. Lin C, Zhong Z, Lok MC, Jiang X, Hennink WE, Feijen J, Engbersen JFJ. Novel bioreducible poly (amido amine)s for highly efficient gene delivery. Bioconjugate Chem. 2007;18:138–45.
13. Fukushima S, Miyata K, Nishiyama N, Kanayama N, Yamasaki Y, Kataoka K. PEGylated polyplex micelles from triblock cationomers with spatially ordered layering of condensed pDNA and buffering units for enhanced intracellular gene delivery. J Am Chem Soc. 2005;127:2810–1.
14. Morris MC, Chaloin L, Méry J, Heitz F, Divita G. A novel potent strategy for gene delivery using a single peptide vector as a carrier. Nucleic Acids Res. 1999;27:3510–7.
15. Morishita N, Nakagami H, Morishita R, Takeda S, Mishima F. Magnetic nanoparticles with surface modification enhanced gene delivery of HVJ-E vector. Biochem Biophys Res Commun. 2005;334:1121–6.
16. Liu Z, Winters M, Holodniy M, Dai H. siRNA delivery into human T cells and primary cells with carbon-nanotube transporters. Angew Chem. 2007;119:2069–73.
17. Srinivasan C, Lee J, Papadimitrakopoulos F, Silbart LK, Zhao M, Burgess DJ. Labeling and intracellular tracking of functionally active plasmid DNA with semiconductor quantum dots. Mol Ther. 2006;14:192–201.
18. Christou P, McCabe DE, Martinell BJ, Swain WF. Soybean genetic engineering-commercial production of transgenic plants. Trends Biotechnol. 1990;8:145–51.
19. Olton D, Li J, Wilson ME, Rogers T, Close J, Huang L, Kumta PN, Sfeir C. Nanostructured calcium phosphates (NanoCaPs) for non-viral gene delivery: influence of the synthesis parameters on transfection efficiency. Biomaterials. 2007;28:1267–79.
20. Yang J, Lee ES, Noh MY, Koh SH, Lim EK, Yoo A. Ambidextrous magnetic nanovectors for synchronous gene transfection and labeling of human MSCs. Biomaterials. 2011;32:6174–82.
21. Liu Y, Chen Z, Gu N, Wang J. Effects of DMSA-coated Fe (3) O (4) magnetic nanoparticles on global gene expression of mouse macrophage RAW264. 7 cells. Toxicol Lett. 2011;28:6174–82.
22. Lei Y, Rahim M, Ng Q, Segura T. Hyaluronic acid and fibrin hydrogels with concentrated DNA/PEI polyplexes for local gene delivery. J Controlled Release. 2011;153:255–61.
23. Sun K, Wang J, Zhang J, Hua M, Liu C, Chen T. Dextran-g-PEI nanoparticles as a carrier for co-delivery of adriamycin and plasmid into osteosarcoma cells. Int J Biol Macromol. 2011;49:173–80.
24. Neu M, Fischer D, Kissel T. Recent advances in rational gene transfer vector design based on poly (ethylene imine) and its derivatives. J Gene Med. 2005;5:992–1009.
25. Ragusa A, García I, Penadés S. Nanoparticles as nonviral gene delivery vectors. IEEE Trans Nanobioscience. 2007;6:319–30.
26. Lübbe AS, Alexiou C, Bergemann C. Clinical applications of magnetic drug targeting. J Surg Res. 2001;95:200–6.
27. Bae KH, Choi SH, Park SY, Lee Y, Park TG. Thermosensitive pluronic micelles stabilized by shell cross-linking with gold nanoparticles. Langmuir. 2006;22:6380–4.
28. Lu J, Ma S, Sun J, Xia C, Liu C, Wang Z, Zhao X, Gao F, Gong Q, Song B. Manganese ferrite nanoparticle micellar nanocomposites as MRI contrast agent for liver imaging. Biomaterials. 2009;30:2919–28.
29. Lee PW, Hsu SH, Wang JJ, Tsai JS, Lin KJ, Wey SP, Chen FR, Lai CH, Yen TC. Sung H W: The characteristics, biodistribution, magnetic resonance imaging and biodegradability of superparamagnetic core-shell nanoparticles. Biomaterials. 2010;31:1316–24.
30. Chen D, Jiang M, Li N, Gu H, Xu Q, Ge J, Xia X, Lu J. Modification of magnetic silica/iron oxide nanocomposites with fluorescent polymethacrylic acid for cancer targeting and drug delivery. J Mater Chem. 2010;20:6422–9.
31. Hong R, Fischer NO, Emrick T, Rotello VM. Surface PEGylation and ligand exchange chemistry of FePt nanoparticles for biological applications. Chem Mater. 2005;17:4617–21.
32. Huang C, Zhou YB, Jin Y, Zhou X, Tang ZM, Guo X, Zhou SB. Preparation and characterization of temperature-responsive and magnetic nanomicelles. J Mater Chem. 2011;21:5660–7.
33. Sun J, Zhou SB, Hou P, Yang Y, Weng J, Li XH, Li MY. Synthesis and characterization of biocompatible Fe_3O_4 nanoparticles. J Biomed Mater Res A. 2007;80:333–41.
34. Kobayashi M, Ryosuke M, Hideyuki O, Atsushi T. Precise surface structure control of inorganic solid and metal oxide nanoparticles through surface-initiated radical polymerization. Sci Technol Adv Mater. 2006;7:617–28.
35. Wang L, Neoh KN, Kang ET, Shuter B, Wang SC. Biodegradable magnetic-fluorescent magnetite/poly(DL-lactic acid-co-a, b-malic acid) composite nanoparticles for stem cell labeling. Biomaterials. 2010;31:3502–11.
36. Kim MS, Chen YF, Liu YC, Peng XG. Super-stable, high-quality Fe_3O_4 dendron-nanocrystals dispersible in both organic and aqueous solutions. Adv Mater. 2005;17:1429–32.
37. Lee JH, Lee KR, Moon SH, Lee YH, Park TG, Cheon JW. All-in-one target-cell-specific magnetic nanoparticles for simultaneous molecular imaging and siRNA delivery. Angew Chem Int Ed. 2009;121:4238–43.
38. Shi S, Guo QF, Kan B, Fu SZ, Wang XH, Gong CY, Deng HX, Luo F, Zhao X, Wei YQ. A novel poly (ε-caprolactone)-pluronic-poly (ε-caprolactone) grafted polyethyleneimine (PCFC-g-PEI), Part 1, synthesis, cytotoxicity, and in vitro transfection study. BMC Biotechnol. 2009;9:65.
39. Lu X, Wang QQ, Xu FJ, Tang GP, Yang WT. A cationic prodrug/therapeutic gene nanocomplex for the synergistic treatment of tumors. Biomaterials. 2011;32:4849–56.
40. Mikhaylova M, Kim DK, Bobrysheva N, Osmolowsky M, Semenov V. Superparamagnetism of magnetite nanoparticles: dependence on surface modification. Langmuir. 2004;20:2472–7.
41. Huang FW, Wang HY, Li C, Wang HF, Sun YX, Feng J, Zhang XZ, Zhuo RX. PEGylated PEI-based biodegradable polymers as non-viral gene vectors. Acta Biomater. 2010;6:4285–95.
42. Xenariou S, Griesenbach U, Ferrari S, Dean P, Scheule R, Cheng S, Geddes D, Plank C, Alton E. Using magnetic forces to enhance non-viral gene transfer to airway epithelium in vivo. Gene Ther. 2006;13:1545–52.